IJST, Transactions of Mechanical Engineering, Vol. 38, No. M2, pp 361-373
Printed in The Islamic Republic of Iran, 2014

A NOVEL HYDRODYNAMIC FOCUSING MICRODEVICE FOR FLOW CYTOMETRY APPLICATIONS*

A. H. VAKILZADEH AND R. KAMALI**

Dept. of Mechanical Engineering, Shiraz University, 71348-51154, Shiraz, I. R. of Iran
Email: rkamali@shirazu.ac.ir

Abstract– Hydrodynamic focusing is one of the most utilized techniques in microfluidics. Its applications have been employed in a wide variety of biological analyses including on-chip flow cytometry, single molecule detection, and laminar mixers. In the present study, a new hydrodynamic focusing microdevice for flow cytometry applications is presented and numerically investigated. In the proposed microdevice, the sample fluid is compressed both in vertical and horizontal directions simultaneously by radial sheath flows injected within flow cytometer through one ring. The microdevice configuration is optimized and effective parameters on stream distribution are investigated. In addition, in order to observe hydrodynamic focusing phenomena, particles trajectories are studied. Moreover, results of the proposed model are compared with the previous one in order to verify that the performance of the present model is more efficient.

Keywords– 3D hydrodynamic focusing, flow cytometry**,** particle trajectory, numerical investigation**,** molecule detection

1. INTRODUCTION

Flow cytometer is one of the most successful applications of microfludic devices that has become quite popular for cell sorting and cell counting analyses [1-4] in fields such as medical diagnostics, bioengineering as well as Micro electro mechanical systems (MEMS) in general.

Flow cytometry is a powerful method to measure the properties of individual particles [5] by suspending them in fluid flow and focusing to the center of the micro channel such that they move in a single file one by one. Different methods are used to focus these particles such as, Narrowing Channel Section [6-8], Electrokinetic Focusing [9-13], Dielectrophoresis Focusing [14-20] and Hydrodynamic Focusing. Electrophoresis and electrokinetic focusing damage the particle membrane. Hence, hydrodynamic focusing is used where 3D focusing is essential.

Hydrodynamic focusing devices have had an important role in flow cytometery. It ensures that particles move through the detector one at a time, along the same path. In early hydrodynamic focusing devices, sample fluids were focused in two steps. A sample flow was focused vertically to a narrow stream by using one or two sheath fluids, then it was horizontally focused to a small core region by using a cross flow.

Yanga et al. [21] have developed a hydrodynamic focusing device in which the sample flow is focused vertically by a slight slanting and horizontal focusing is done by two coaxial sheath flows from the sides.

Chang et al. [22] have designed and fabricated a hydrodynamic focusing device in which the sample flow is first focused vertically to a narrow stream by using two sheath flows, then it is horizontally focused to a small core region by using a cross flow.

*Received by the editors August 23, 2013; Accepted April 30, 2014.
**Corresponding author

Mao et al. [5] have proposed a curved micro channel to use the effect of centrifugal force to focus sample flow further vertically. In their model sample flow was focused in two steps. In the first step it was focused vertically by using a sheath flow and centrifugal force. Then in the second step it was focused horizontally by a pair of sheath flow.

Tsai et al. [23] have presented a three-dimensional hydrodynamic focusing technique with two pairs of sheath flows and a micro-weir structure. In their model, the sample flow is focused in horizontal direction by using a set of sheath flows, then in vertical direction by using another set of sheath flow and a micro-weir structure.

Kim et al. [24] increased the operation of vertical focusing by means of locally increasing the aspect ratio of thickness to width of the side channels. Two sheath flows, A and B, focus the sample flow in the vertical direction via the locally increased aspect ratio. Then it is focused horizontally by the sheath flow, C, (Fig. 1a).

Tony [25] has recently increased the performance of hydrodynamic focusing devices by changing the location of side channels. In this research, the COMSOL software was utilized for the flow simulation.

Zhang et al. [26] have also designed and fabricated a hydrodynamic focusing device. In their model two smaller channels are fabricated in the upper layer and two larger channels are fabricated in the lower layer. Sample flow is driven through B and sheath flows are driven through A, C and D. The focusing of the sample at the end tip seems to be rectangular shape, which is not very efficient (Fig. 1b).

In this paper, a new hydrodynamic focusing microdevice is presented. Unlike previous works in which sample fluid was first focused in the vertical direction with one or two sheath fluids and another sheath fluid was introduced for converging the sample stream in the horizontal direction (or vice versa), the present device focuses the sample fluid in both the vertical and horizontal directions simultaneously and more efficiently.

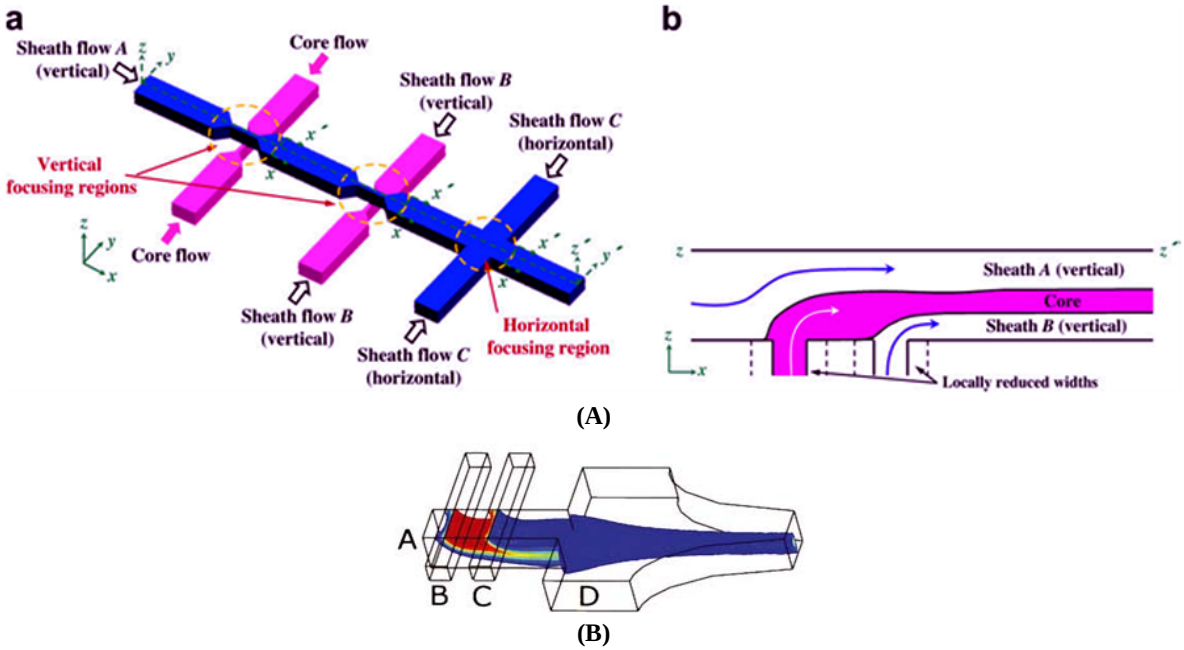

Fig. 1. Schematic diagram of hydrodynamic focusing device proposed with **(A)** Kim et al. [24] (a) overall view and (b) vertical view **(B)** Zhang et al. [26]

Figure 2 shows the geometry of hydrodynamic focusing device proposed in this study. This device is designed after numerically investigating several models. It consists of two parts, channel A as a main channel with 120 μm in width and height and ring B with 150 μm in radius and 40 μm in width.

Sample flow is driven through channel A with a velocity V_A for focusing and sheath flows are driven radially through ring B with a velocity V_B to focus the sample flow in both vertical and horizontal directions.

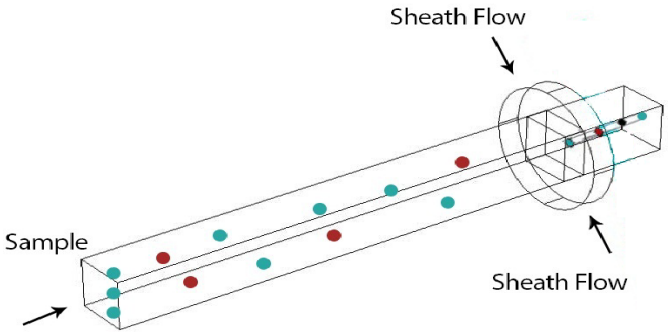

Fig. 2. Geometry of hydrodynamic focusing device proposed in this study

2. NUMERICAL ANALYSIS MODEL

The grid system used in this numerical analysis is shown in Fig. 3. As illustrated, about 84000 tetrahedral elements are used in the entire domain.

Grid independence check is performed using four values of mesh size to ensure the solution does not depend on the mesh. Numerical computation is performed using 40e3 elements, 84e3 elements, 155e3 elements and 231e3 elements.

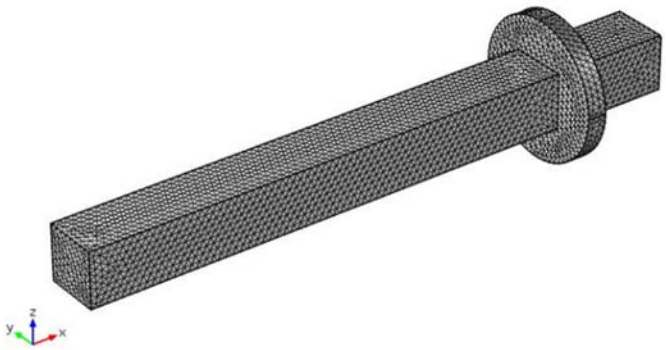

Fig. 3. Geometry with 84e3 tetrahedral elements

Figure 4 shows vertical focusing with respect to height of microchannel at V_A=150 µm/s and V_B=1000 µm/s. As it can be seen, the trend of diagrams with 84e3 elements, 155e3 elements and 231e3 elements are similar to each other. This allowed us to choose the grid system with about 84e3 elements. Before performing simulation on the proposed model, the model of Tony [25] is simulated and the obtained results are compared to his study. In his model, sample flow is driven through channel *A* with velocity V_A=500 µm/s and a pair of sheath flows are driven through channels *B* and *C* with velocities V_B=V_C=1200 µm/s to focus sample flow in vertical direction, then a pair of sheath flows are driven through channel *D* with V_D=15 µm/s to the focus sample horizontally. In order to validate the numerical method, a diagram showing horizontal focusing with respect to the width of microchannel is drawn in Fig. 5. As it can be seen, the present results have good agreement with results obtained from Tony [25].

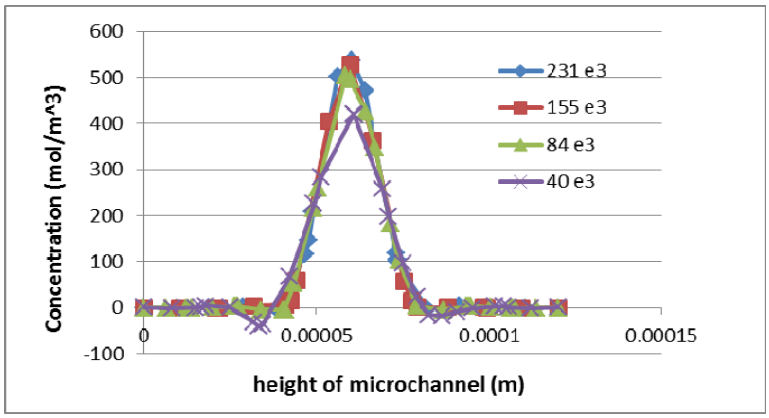

Fig. 4. Vertical focusing with respect to height at V_A=150 µm/sec, V_B=1000µm/sec

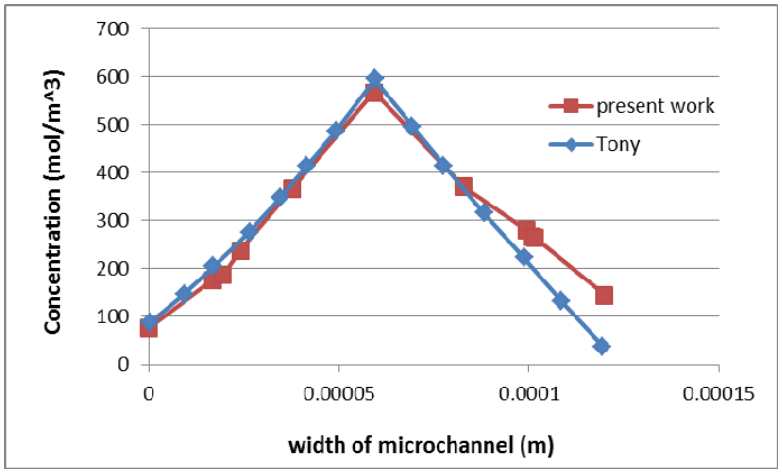

Fig. 5. Horizontal focusing with respect to width of microchannel

This study conducted a numerical analysis of performance of the hydrodynamic focusing device with regard to the changes in three variables, i.e., the flow velocity ratio, thickness and radius of ring B, which have the greatest impact on the focusing of sample flow.

Finite elements code is used to study behavior of the sample and sheath flows, particle tracing and concentration of species. The flow in device is assumed to be steady-state, laminar and incompressible.

Continuity and momentum equations are used to observe the fluid flow. Moreover, convection and diffusion equations are employed to observe the amount of species concentration in the hydrodynamic focusing device.

Because L and u are relatively smaller, the Reynolds number is lower than unity. Therefore, the flow can be approximated as a creeping flow and there is less chance for mixing. Thus, the continuity, stokes, convection and diffusion equations are used for the numerical simulation. These equations are as follows:

$$\nabla.u = 0 \tag{1}$$

$$\nabla.\left[-pI + \mu\left(\nabla u + (\nabla u)^T\right)\right] + F = 0 \tag{2}$$

$$\nabla.\left(-D_i \nabla c_i\right) + u.\nabla c_i = R_i \tag{3}$$

where, **u** is the velocity vector, p is the pressure, **F** is body force, D_i is the diffusion coefficient, c_i is the concentration of species i and R_i is the reaction.

Fluid flow at the inlet of channel A is set as laminar and fully developed and at the other inlet is set as normal inflow.

Water with ρ=1e3 (kg/m^3) and μ=1.803e-3 (Pa.s) as sample fluid and *diluted glycerol* with ρ=1e3(kg/m^3) and μ=1.002e-3 (Pa.s) as sheath fluid are chosen. Diffusion coefficient and input concentration are set to 1e-10 (m^2/s) and 500 (mol/m^3), respectively.

3. NUMERICAL RESULTS

a) Effect of flow velocity ratio on stream width

In order to investigate the effect of flow velocity ratio on stream width, the inlet velocity of sample is kept at V_A=150 µm/s and the velocities of sheath flows are changed from 150 µm/s to 1800 µm/s. (i.e. K= V_B/ V_A is varied from 1 to 12.)

Figure 6 shows the effect of velocity of sheath and sample flows on stream distribution within flow cytometer under different flow velocity ratios. It can be seen that sample flow is compressed in horizontal direction with sheath flow and the focused stream width becomes narrower by increasing flow velocity ratio.

Figure 7 shows the sample concentration along y-axis at cross sectional located 1200 µm (i.e. 200 µm upstream of ring B) under different flow velocity ratios. As it can be seen, the focused sample stream decreases by increasing flow velocity ratio. Moreover, the sample concentrations under K= V_B/V_A=9 and V_B/V_A=12 not only have the same trend but also they are virtually overlapped. On the other hand, the focused sample stream does not depend on the flow velocity ratio for K>9, this result logically agrees with the experimental result of Fu et al. [27]. Hence, the proposed device can focus the sample flow horizontally very well for K=9.

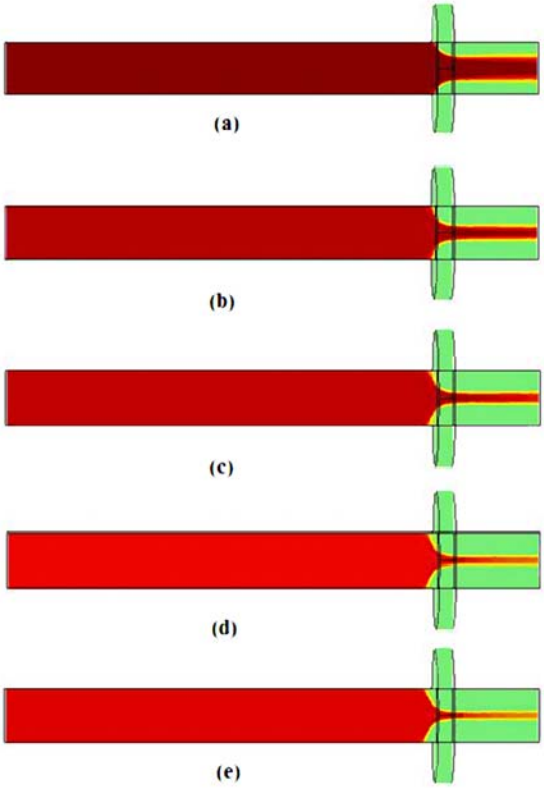

Fig. 6. Simulation of the hydrodynamic focusing of sample in horizontal direction under flow velocity ratios of: a 1:1, b 1:4, c 1:8, d 1:12 and e 1:16

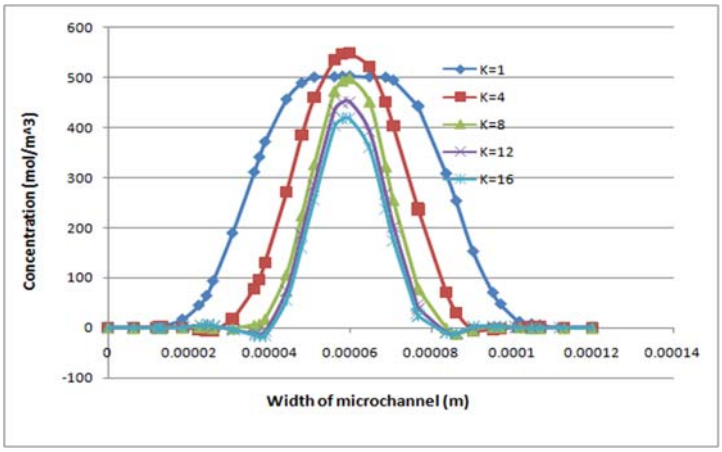

Fig. 7. Horizontal focusing with respect to width of microchannel under flow velocity ratios of: **a** 1:1, **b** 1:4, **c** 1:8, **d** 1:12 and **e** 1:16

b) Effect of radius of ring B

Cross sectional distribution of sample flow under different flow velocity ratios with different radius of ring B are numerically obtained and presented in Fig. 8. Here, R is radius of ring B. As it can be seen, the total momentum of the sheath flow increases with increasing radius of ring B from 130 µm to 170 µm so that the sample height decreases. Moreover, it shows that the height of sample is fairly the same at R=150 µm and R=170 µm. Figure 9 confirms this claim and shows that the relative focused stream heights at R=150 µm and R=170 µm are overlapped. Therefore, R=150 µm is the optimal radius for ring B.

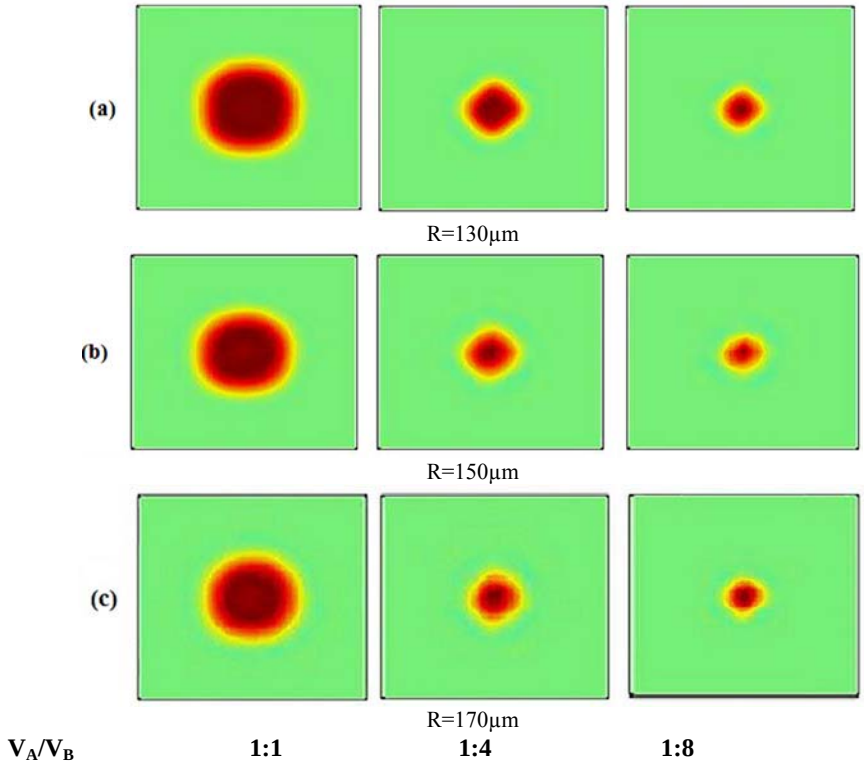

Fig. 8. Simulation results obtained for sample stream distribution for different flow velocity ratios and radius of: (a) R=130 µm, (b) R=150 µm, (c) R=170 µm

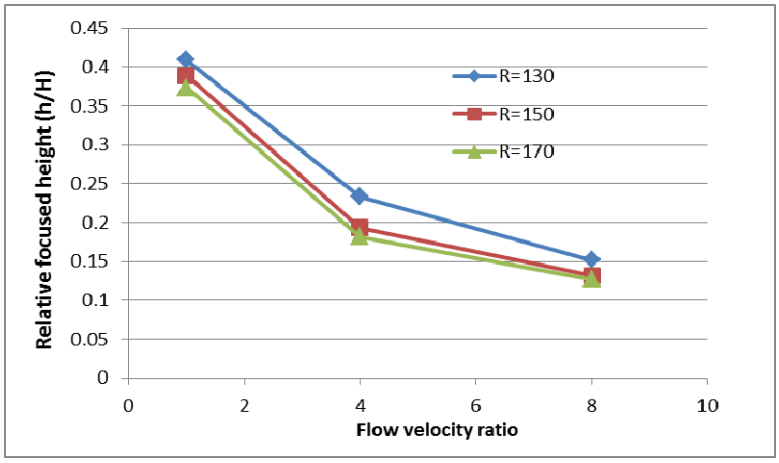

Fig. 9. Variation of relative focused height of sample with respect to flow velocity ratio for R=130, 150 and 160 µm

c) Effect of thickness of ring B3

In order to investigate the effect of thickness of ring B, cross sectional distribution of sample flow under different flow velocity ratios with different thicknesses of ring B are numerically obtained and presented in Fig. 11. Here, W is the thickness of ring B. The figure shows that the further the thickness of ring B, the narrower the focused stream.

The variation of focused stream height with flow velocity ratios for different thicknesses of ring B is shown in Fig. 10. As it can be seen, it decreases by increasing W. In addition, numerical results of W= 50µm and W= 60µm are virtually the same. Hence, W= 50 µm is the optimal thickness for ring B. It is more cost-effective than W=60 µm.

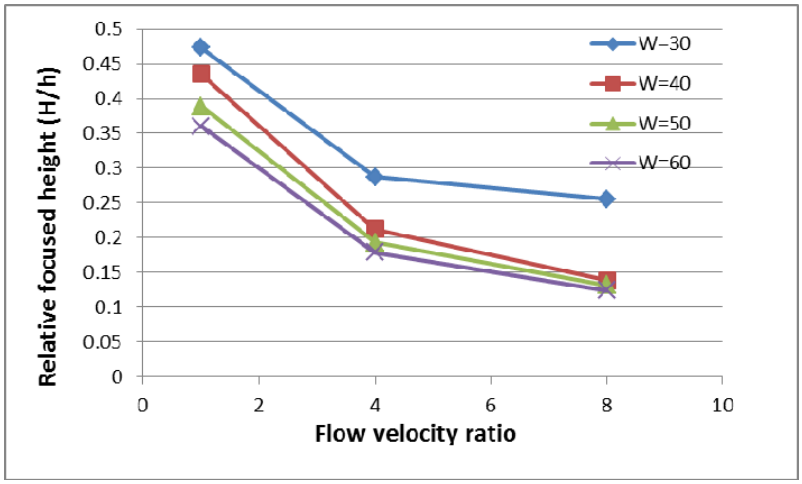

Fig. 10. Variation of relative focused height of sample with respect to flow velocity ratio for W=30, 40, 50 and 60

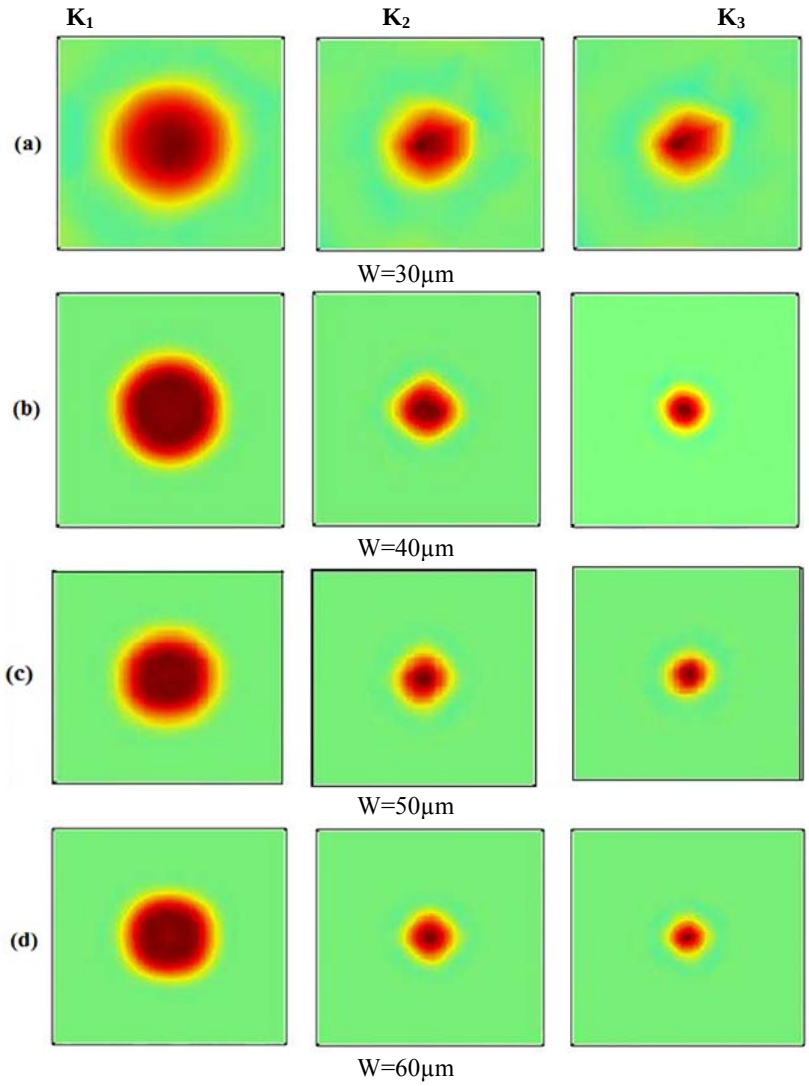

Fig. 11. Simulation results obtained for sample stream distribution for different flow velocity ratios and thickness of : (a) W=30 μm, (b) W=40 μm (c) W=50 μm and (d) W=60 μm

4. PARTICLES TRAJECTORIES

The performance of a hydrodynamic focusing device is perceived by tracking the particle and studying if they are focused enough so that they pass under the detector one by one in a single file. The Eulerian-Lagrangian method is used to simulate the particles trajectory. In this paper, the motion of particles with diameter d_p=1μm and density ρ_p=1050 Kg/m^3 at velocity condition V_A=150μm/s and V_B=1400μm/s is studied. Brownian force is neglected because the diameter of is larger than 0.01 μm. The drag and gravitational forces are used to simulate the particle trajectory. The governing equation for the particle trajectory can be described by the Newton's second law:

$$\frac{d\left(m_p v\right)}{dt} = \frac{1}{\tau_p} m_p \left(u - v\right) + m_p g \frac{\left(\rho_p - \rho\right)}{\rho_p} \tag{4}$$

$$\tau_p = \frac{\rho_p d_p^{\,2}}{18\mu} \tag{5}$$

where **u** is the local fluid velocity vector, **v** is particle velocity and μ is fluid dynamic viscosity.

In order to study the trajectory of the particles, 4 particles are simultaneously released into sample flow from positions that are described below:

Particle 1: x=0, y= 2e-5, z=-2e-5 Particle 3: x=0, y=-2e-5, z=-2e-5
Particle 2: x=0, y= 2e-5, z= 2e-5 Particle 4: x=0, y=-2e-5, z= 2e-5
(Coordinate origin is at the center of the inlet of channel A)

Figure 12 shows the position of particles at the inlet (at t=0) and at the end of micro channel (where all of them are focused). Moreover, particle locations in the micro channel are shown in Fig. 13. In addition, the positions of two particles on the Y-X and Z-X planes along the channel are shown in Fig. 14. Here, the particles are injected from distance of 2.5e-5 m and -2.5e-5 m from the center along Z- axis.

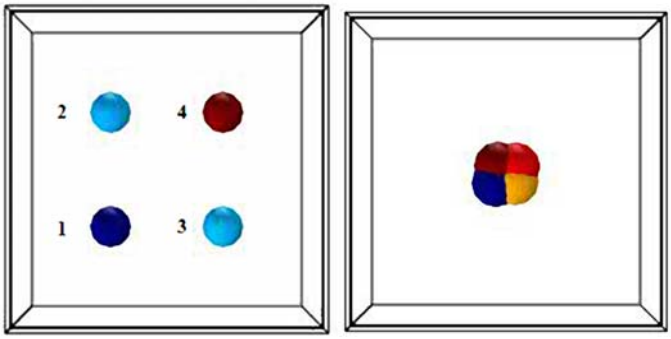

(a) (b)

Fig. 12. Particle location **(a)** at inlet **(b)** at the end of micro channel

Figure 13 shows that, when the particles are affected by sheath flow, they are focused and flow in a single file through the device.

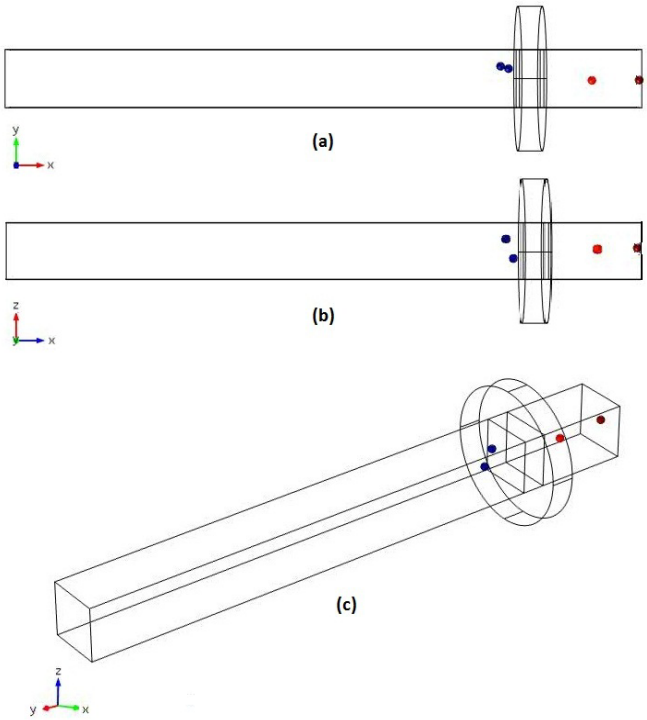

Fig. 13. Numerical trace results of microparticle of diameter 10 micron
(a) in X-Y plane (b) in X-Z plane (c) overall view

Figure 14 shows that, as two particles arrive at focusing unit they are affected by higher velocity of sheath flow and tend to move towards the center line of the channel. Besides, it can be seen that both particles have the same track in focusing unit.

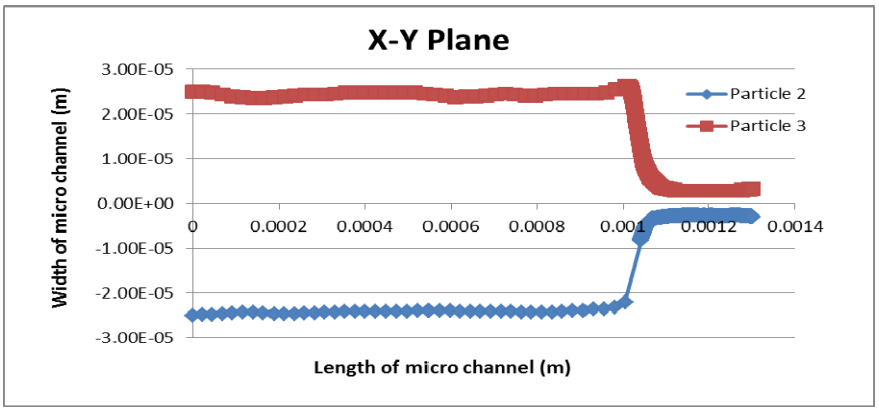

(a)

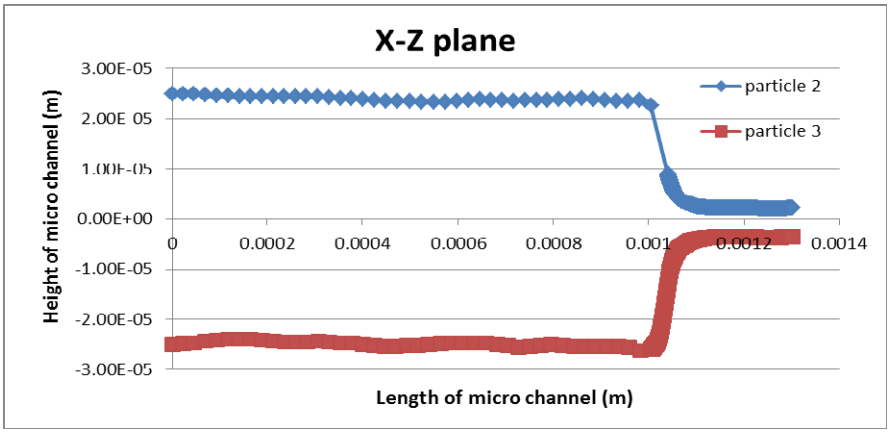

(b)

Fig. 14. Particle position along the channel **(a)** in Y-X plane **(b)** in Z-X plane

5. COMPARISON BETWEEN THE PROPOSED MODEL AND THE PREVIOUS RESULT

In order to compare this device with the previous one, the horizontal and vertical focusing with respect to the width/height at the end of microchannel as well as the concentration contour for the proposed device and the previous one [27] are shown in Fig. 15 and 16, respectively. As it can be seen, the focused width in the present device is narrower than the previous one. In addition, the present device not only has a maximum concentration at the center of the microchannel but also within 45 μm from the center of micro channel in horizontal and vertical directions, the concentration is zero. This means that the current device focuses the sample flow at the center of the microchannel much better than the previous one. According to Fig. 15a, contrary to the previous device, this device focuses the sample flow both in horizontal and vertical direction identically. On the other hand, the graph of horizontal focusing is identical with the vertical focusing, completely overlapping each other.

Figure 16 shows the concentration in the entire domain and at the end of microchannel. It is evident that the performance of the present device is much better than the previous one. Furthermore, the focusing of the sample at the end tip has a circular shape which is much more efficient.

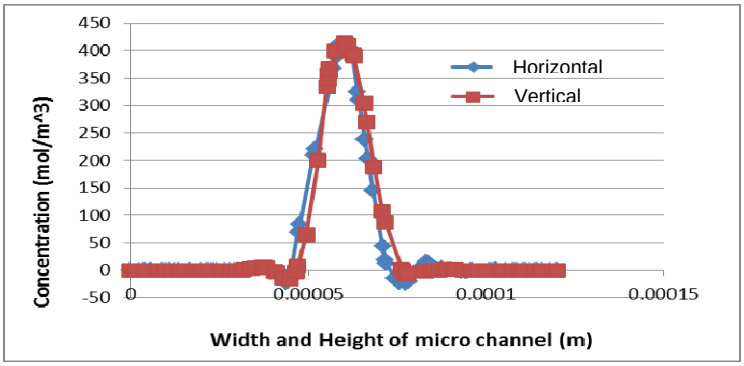

(a)

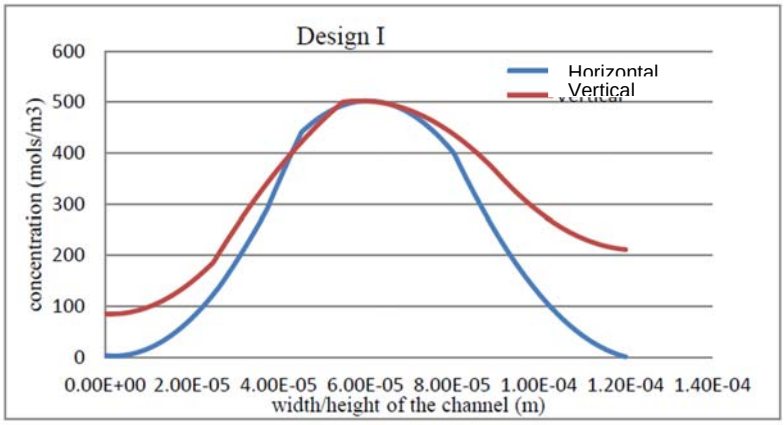

(b)

Fig. 15. Horizontal and vertical focusing with respect to width/height (a) new device (b) previous device, Tony [25]

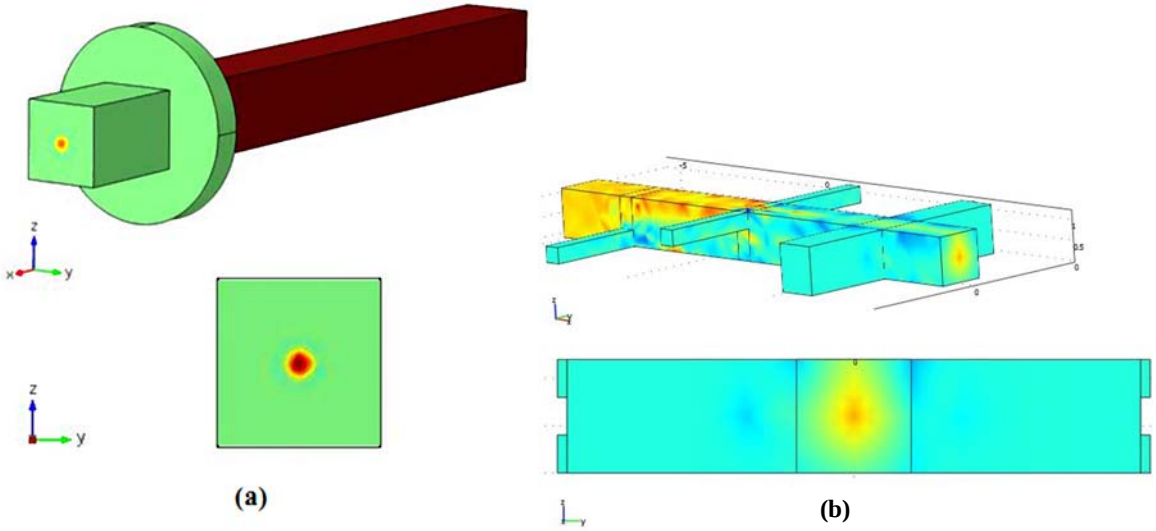

Fig. 16. (a) Presented new device (b) numerical simulation results of 3D hydrodynamic focusing for previous device, Tony [25]

6. CONCLUSION

In this paper, a novel three dimensional hydrodynamic focusing microdevice has been proposed and numerically investigated. The effect of sheath flow velocity on focusing width is also investigated and it is

shown that for $V_B/V_A>12$ the focused width does not strongly depend on sheath flow velocity. Moreover, the effect of radius and thickness of ring B is studied and it is shown that R=150 μm and W=50μm is the optimal radius and thickness for the proposed device. In addition, 4 particles are released into the sample flow from different locations and their trajectories are explored. It is shown that when the particles arrive at the focusing unit, they are focused very well and flow in a single file through the device. Besides, it is shown that the microdevice is capable of focusing the sample flow in just one step. The concentration at the end of the micro channel and the particles trajectories in the micro channel are numerically modeled. Furthermore, it is shown that the focusing of the sample at the end tip of the microdevice is circular in shape making it much more efficient.

REFERENCES

1. Huh, D., Gu, W., Kamotani, Y., Grotberg, J. B. & Takayama, S. (2005). Microfluidics for flow cytometric analysis of cells and particles. *Physiol Meas*, Vol. 26, No. 3, pp. 73-98.
2. Brown, M. & Wittwer, C. (2000). Flow cytometry: principles and clinical applications in hematology. *Clin Chem*, Vol. 46, No. 8, pp. 1221-1229.
3. Wang, M. M., Tu, E., Raymond, D. E., Yang, J. M., Zhang, H., Hagen, N. and et al. (2004). Microfluidic sorting of mammalian cells by optical force switching. *Nat Biotechnol*, Vol. 23, No. 1, pp. 83-87.
4. Wolff, A., Perch-Nielsen, I. R., Larsen, U., Friis, P., Goranovic, G., Poulsen, C. R., et al. (2003). Integrating advanced functionality in a microfabricated high-throughput fluorescent-activated cell sorter. *Lab Chip*, Vol. 3, No. 1, pp. 22-27.
5. Mao, X., Waldeisen, J. R. & Huang, T. J. (2007). [rising dbl quote] Microfluidic drifting-implementing three-dimensional hydrodynamic focusing with a single-layer planar microfluidic device. *Lab on a Chip*, Vol. 7, No. 10, pp. 1260-1262.
6. Takeuchi, S., Garstecki, P., Weibel, D. B. & Whitesides, G. M. (2005). An Axisymmetric Flow-Focusing Microfluidic Device". Adv Mater, 17(8), pp. 1067-1072.
7. Chau, L. K., Osborn, T., WU, C.C. & Yager, P. (1999). Microfabricated silicon flow-cell for optical monitoring of biological fluids. *Analytical sciences*, Vol. 15, No. 8, pp. 721-724.
8. Fu, A. Y., Spence, C., Scherer, A., Arnold, F. H. & Quake, S. R. (1999). A microfabricated fluorescence-activated cell sorter. *Nat Biotechnol*, Vol. 17, No. 11, pp. 1109-1111.
9. Church, C., Zhu, J., Wang, G., Tzeng, T. R. J. & Xuan, X. (2009). Electrokinetic focusing and filtration of cells in a serpentine microchannel. *Biomicrofluidics*, Vol. 3, 044109.
10. Fu, L. M., Yang, R. J. & Lee, G. B. (2003). Electrokinetic focusing injection methods on microfluidic devices. *Anal Chem*, Vol. 75, No. 8, pp. 1905-1910.
11. Schrum, D. P., Culbertson, C. T., Jacobson, S. C., Ramsey, J. M. (1999). Microchip flow cytometry using electrokinetic focusing. *Anal Chem*, Vol. 71(19), pp. 4173-4177.
12. Jacobson, S. C. & Ramsey, J. M. (2000). Microfabricated device and method for multiplexed electrokinetic focusing of fluid streams and a transport cytometry method using same.
13. Fu, L. M., Yang, R. J., Lin, C. H., Pan, Y. J. & Lee, G. B. (2004). Electrokinetically driven micro flow cytometers with integrated fiber optics for on-line cell/particle detection. *Anal Chim Acta*, Vol. 507, No. 1, pp. 163-169.
14. Takahashi, T., Ogata, S., Nishizawa, M. & Matsue, T. (2003). A valveless switch for microparticle sorting with laminar flow streams and electrophoresis perpendicular to the direction of fluid stream. *Electrochemistry communications*, Vol. 5, No. 2, pp. 175-177.
15. Lin, C. H., Lee, G. B., Fu, L. M. & Hwey, B. H. (2004). Vertical focusing device utilizing dielectrophoretic force and its application on microflow cytometer. *Microelectromechanical Systems*, Vol. 13, No. 6, pp. 923-932.

16. Cheng, I. F., Chang, H. C., Hou, D. & Chang, H. C. (2007). An integrated dielectrophoretic chip for continuous bioparticle filtering, focusing, sorting, trapping, and detecting. *Biomicrofluidics*, Vol. 10, No. 1(2): 021503.
17. Zhu, J. & Xuan, X. (2009). Dielectrophoretic focusing of particles in a microchannel constriction using DC-biased AC flectric fields. *Electrophoresis*, Vol. 30, No. 15, pp. 2668-2675.
18. Cheng, I. F., Chung, C. C. & Chang, H. C. (2011). High-throughput electrokinetic bioparticlefocusing based on a travelling-wavedielectrophoretic field. *Microfluidics and nanofluidics*, pp. 1-12.
19. Yu, C., Vykoukal, J., Vykoukal, D. M., Schwartz, J. A., Shi, L. & Gascoyne, P.R.C. (2005). A three-dimensional dielectrophoretic particle focusing channel for microcytometry applications. *icroelectromechanical Systems*, Vol. 14, No. 3, pp. 480-487.
20. Holmes, D., Morgan, H. & Green, N. G. (2006). High throughput particle analysis: Combining dielectrophoretic particle focussing with confocal optical detection. *Biosensors and Bioelectronics*, Vol. 21, No. 8, pp. 1621-1630.
21. Yang, R., Feeback, D. L. & Wang, W. (2005). Microfabrication and test of a three-dimensional polymer hydro-focusing unit for flow cytometry applications. *Sensors and Actuators A: Physical*, Vol. 118, 2, pp. 259-267.
22. Chang, C. C., Huang, Z. X. & Yang, R. J. (2007). Three-dimensional (PDMS) microchannels hydrodynamic focusing in two-layer polydimethylsiloxane, *Micromech Microengineering*, Vol. 17, pp. 1479-1486.
23. Tsai, C. H., Hou, H. H. & Fu, L. M. (2008). An optimal three-dimensional focusing technique for micro-flow cytometers. *Microfluidics and nanofluidics*, Vol. 5, No. 6, pp. 827-836.
24. Kim, D. S., Kim, D. S. D., Han, K. & Yang, W. (2009). An efficient 3-dimensional hydrodynamic focusing microfluidic device by means of locally increased aspect ratio. *Microelectronic Engineering*, Vol. 86, No. 4-6, pp. 1343-1346.
25. Tony, A. (2011). Design of a microfluidic chip for three dimensional hydrodynamic focusing in cell cytometry applications. M.Sc. Thesis, Concordia University, Montreal, Canada.
26. Zhang, G, Jensen, T. G. & Kutter, P. J. (2012). Detection of unlabeled particles in the low micrometer size range using light scattering hydrodynamic3D focusing microfluidic system. *Electrophoresis*, pp. 1715-1722.
27. Fu, L. M., Tsai, C. H. & Lin, C. H. (2008). A high-discernment micro-flow cytometer with micro-weir structure. Electrophoresis, Vol. 29, No. 9, pp. 1874-1880.